Materials Today Advances 7 (2020) 100077

Contents lists available at ScienceDirect

Materials Today Advances

journal homepage: www.journals.elsevier.com/materials-today-advances/

Forming of metallic glasses: mechanisms and processes

Z. Li, Z. Huang, F. Sun, X. Li, J. Ma*

Guangdong Provincial Key Laboratory of Micro/Nano Optomechatronics Engineering, College of Mechatronics and Control Engineering, Shenzhen University, Shenzhen 518060, PR China

ARTICLE INFO

Article history:
Received 25 March 2020
Accepted 20 April 2020
Available online 11 June 2020

Keywords:
Metallic glass processing
Thermoplastic forming
Ultrasonic-assisted forming
Plastic behavior

ABSTRACT

Metallic glasses (MGs) with amorphous structures and tunable compositions have been considered excellent structural and functional materials, especially in the frontier fields of microelectromechanical systems (MEMS), biomedical engineering, energy conversion, etc. Making these materials into desired structures for different applications has always been one of the research focuses in the past decades. Due to high strength and poor plasticity at ambient temperature, MGs are difficult to be formed and manufactured by conventional approaches. Thermoplastic forming, utilizing the superplasticity property of MGs in supercooled liquid region, has been developed to fabricate micro-/nanofeatures. However, the thermal effect inevitably increases the risks of crystallization and oxidation of MGs during forming, leading to material performance degradation and limiting the process feasibility to specific composition systems of MGs. In view of this, a novel strategy proposed recently is to promote plastic deformation and forming of MGs by high frequency ultrasonic vibration at room temperature, which promises to avoid the shortcomings in thermal forming and extend the forming processes of MGs. In this review article, we would like to first discuss the forming mechanisms of supercooled MGs liquid, the joining of MGs and a variety of fabricated structures based on thermoplastic forming. After that, a concept of ultrasonic-assisted forming of MGs is introduced focusing on plastic behavior under high frequency vibration and the latest process advances including shear punching and manufacturing. Finally, the existing problems and the development prospects will be discussed to facilitate the further researches on MGs forming.

1. Introduction

Metallic glasses (MGs) also called amorphous alloys, with atomic structure of long-range disorder and short-range order, have superior properties such as high strength, high elastic limit and excellent corrosion resistance, etc. [1] Since the 1960s when MG films were first fabricated [2], these unique metals have attracted extensive research interest; different fabrication methods were successively developed including liquid forging [3], fluxing melting [4], mold casting [5], and mechanical alloying [6], significantly improving the critical size of MGs to 80 mm [7]. Good glass forming abilities are essential for MGs based on different compositions to be made in bulk scale. At present, the bulk metallic glasses (BMGs) are generally prepared by rapidly quenching of the molten metal with a sufficiently steep cooling rate (e.g. 10^6 K/s) to avoid the nucleation and crystallization and obtain the glassy state. A series of synthesis rules of MGs were proposed to tune the material compositions in a broad range based on the elements like lanthanum (La), magnesium (Mg), zirconium (Zr), copper (Cu), iron (Fe), palladium (Pd), titanium (Ti), etc [8–10]. It was found that the higher degree of element multiplicity can enhance the structural disorder of MGs, which benefits to improve the glass formation ability [11]. Therefore, utilizing the material features of amorphous structure and flexible compositions, various kind of BMGs have been developed with special functions such as catalysis [12], antibiosis [13], biocompatibility [14], etc. For practical applications, it is also important to form these advanced materials into multiscale structures based on the inherent materials properties.

Comparing to the crystalline metals, MGs has no grain boundaries and crystal dislocation defects, which can theoretically extend the minimum forming size limit and improve the forming quality as well as forming accuracy. However, BMGs generally exhibit poor ductility and formability at room temperature, due to the plastic deformation tending to be localized in sharp shear bands [15,16]. To overcome these limitations, thermoplastic forming (TPF) has been developed to first heat BMGs up to a temperature above the glass-transition temperature (*Tg*) and below the crystallization

* Corresponding author.
E-mail address: majiang@szu.edu.cn (J. Ma).

https://doi.org/10.1016/j.mtadv.2020.100077

temperature (*Tx* so that the materials can relax into supercooled liquid region (SCLR) with a low viscosity, which is suitable for the subsequent thermo-mechanical processes of BMGs such as hot embossing [17], extrusion [18], rolling [19], injection [20] and blow molding [21], etc. By taking advantage of the superplastic flow behavior in SCLR, the forming dimension limit of BMGs can reach to sub-10 nm [22]. This indicates that multitudinous structures can be made from amorphous alloys rather than crystalline metals by TPF under relatively low pressure and temperature. Though the thermal approaches are now widely adopted in the BMGs forming, there were still many challenges considering the forming qualities. It is crucial to retain the amorphous structures and original material properties of BMGs after forming. To reduce the risks of crystallization, the BMGs subjected to TPF generally need have a broad SCLR to provide the sufficient process window [23], which confined TPF to a few kinds of BMGs with specific compositions. The oxidation [24] and chemical segregation [25] of the formed MGs structures are other problems that have always been of concern due to the thermal effect in TPF. Some strategies, for instance, increasing the heating rate [26–28] or reducing the processing time during TPF have been proposed to avoid crystallization and avoid oxidation, while the effective implementation of these strategies need further researches on superplastic flow and forming mechanisms of BMGs in TPF.

To bypass the thermal effect in BMG forming, extensive studies have been devoted to the plastic deformation mechanism at room temperature and the new methods for improving the ductility of BMGs. The classic dislocation slip theory for crystalline metals is not suitable for describing the deformation process of the amorphous alloy without grain boundaries and dislocations. Although the plastic deformation behaviors of amorphous structure are not fully understood, the models of free volume [29] and shear transformation zone (STZ) [30,31] have been proposed to explain the metal atoms re-arrangement during the plastic deformation of BMGs. It is considered that the plastic deformation of BMGs is always accompanied by the generation and annihilation of free volume, and the fracture during deformation is mainly induced by localized shear zone [32]. Based on these theories, several approaches to improve the ductility of BMGs have been carried out. One of the effective ways is to apply constrained loadings on workpiece, such as subjecting it to three dimensional stress [33]; to suppress the generation of shear bands; and increase the free volume in the deformation area, while the desired structures cannot be formed by this method because of the loading constraints. Besides, the softening effect of BMGs recently has been discovered under the high frequency alternating stress [34,35], thus a new method has been developed using ultrasonic vibration to significantly plasticize and form BMGs at ambient temperature. Without the heating process, this ultrasonic-assisted forming method is applicable to BMGs with broader range of compositions and can minimize the thermal defects like crystallization and oxidation. More processes for BMGs forming need be explored to solve diverse demands in practical applications. In this article, as shown in Fig. 1, the developments of TPF for BMGs are comprehensively reviewed including the forming mechanisms in SCLR, the joining of BMGs and the fabrication of micro-/nanostructures. In addition, a promising forming technology is discussed on the plastic behavior of BMGs under high frequency vibration and the up-to-date progress of ultrasonic-assisted forming.

2. Thermoplastic forming

2.1. Forming mechanisms in supercooled liquid region

The unique superplasticity within the SCLR makes metallic glasses the ideal materials for precise and net-shaping of various geometries by thermoplastic forming, which breaks through the limitations of poor processability of BMGs at ambient temperature. It is a complex thermodynamic process since TPF involving material rheology and structure formation kinetics, and the TPF parameters such as stress, temperature, processing time and strain rate tend to have coupled influences on the BMGs formability. Therefore, the understanding of material flowing characteristic and filling mechanism as well as their correlation is crucial to control the thermal plastic formability of the supercooled metal liquid and achieve desired forming quality in the TPF of BMGs.

Previous studies have found that low viscosity and long processing time of BMGs in SCLR benefit in fully filling and improving the formability during the replication of structures from molds [36,37]. In addition to the dependence on inherent property determined by compositions, the viscosity of the supercooled metal liquid also significantly affected by the processing parameters. Experiments showed that remarkable decrease of viscosity of BMGs in SCLR can be obtained under high forming temperature [38] and strain rate [39]. However, according to the crystallization kinetics of BMGs [40–42], the enhancement of atoms diffusion due to low viscosity under high temperature may cause transition of atomic structure from metastable amorphous state to the ordered crystalline state, losing the original properties of BMGs. A general solution for this contradiction in TPF is to establish the time-temperature-transformation (TTT) curves for the specific BMGs through isothermal crystallization experiments [43], guiding for the selection of matched processing time and temperatures in the amorphous regime. In order to achieve optimal processing time window in the TTT curve, more efficient heating methods have been explored to reduce the uniform time ahead of heating and leave sufficient time for the thermal filling and forming in SCLR. A rapid capacitive discharge heating approach with rates of 10^6 K/s was developed for BGMs in the TPF to span the undercooled liquid region [26], which can bypass the crystalline regime and extend the range of effective processing parameters. Another controllable and rapid forming approach were developed based on resistance welding, the high heating power and loading beforehand on the BMGs ensure the heating and forming processes can be finished simultaneously in 150 ms [28], and the forming structures manifested that the rapid processes are conducive to avoid crystallization and degradation in material performance. At certain forming stress and temperature, the increase of strain rate exerting on BMGs during TPF can significantly reduce the viscosity of supercooled liquid while the flow characteristics may undergo transition from Newtonian to non-Newtonian behavior [39], affecting the filling mechanisms and formability. A TPF map that describes the correlation of the BMGs flow characteristics and processing conditions was proposed [44], demonstrating that Newtonian flow obtained at relatively high temperature and low strain rate facilitates filling ability, whereas the replication of mold during forming becomes more difficult at the non-Newtonian flow regime and the mold cavities tend to be partially filled or even not filled due to the inhomogeneous flow as the increase of forming stress and strain rate.

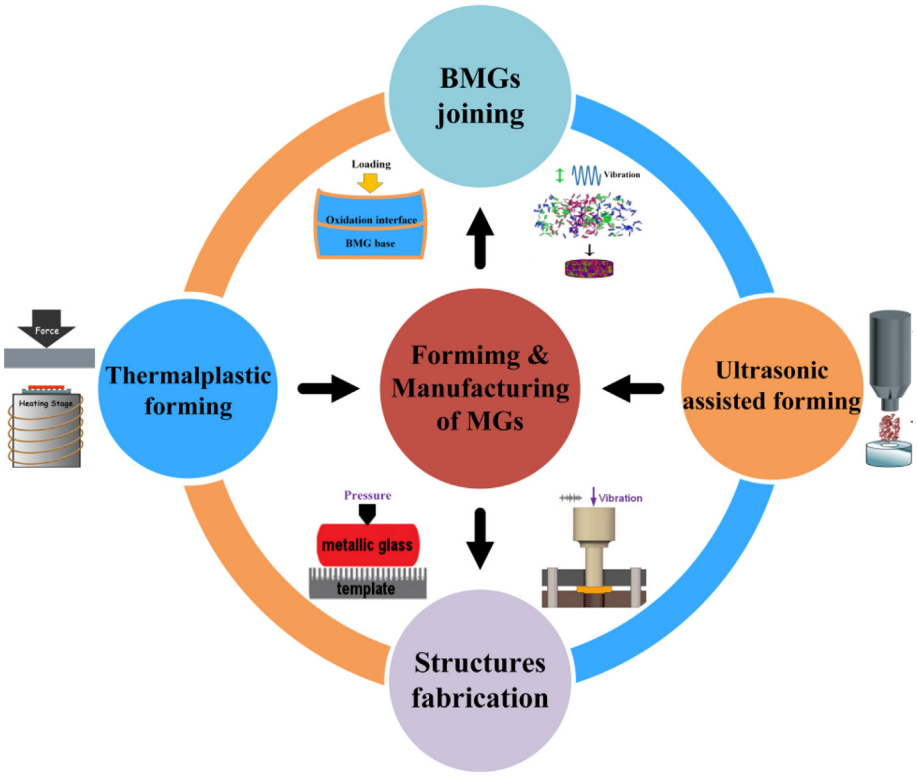

Fig. 1. overview of metallic glasses forming.

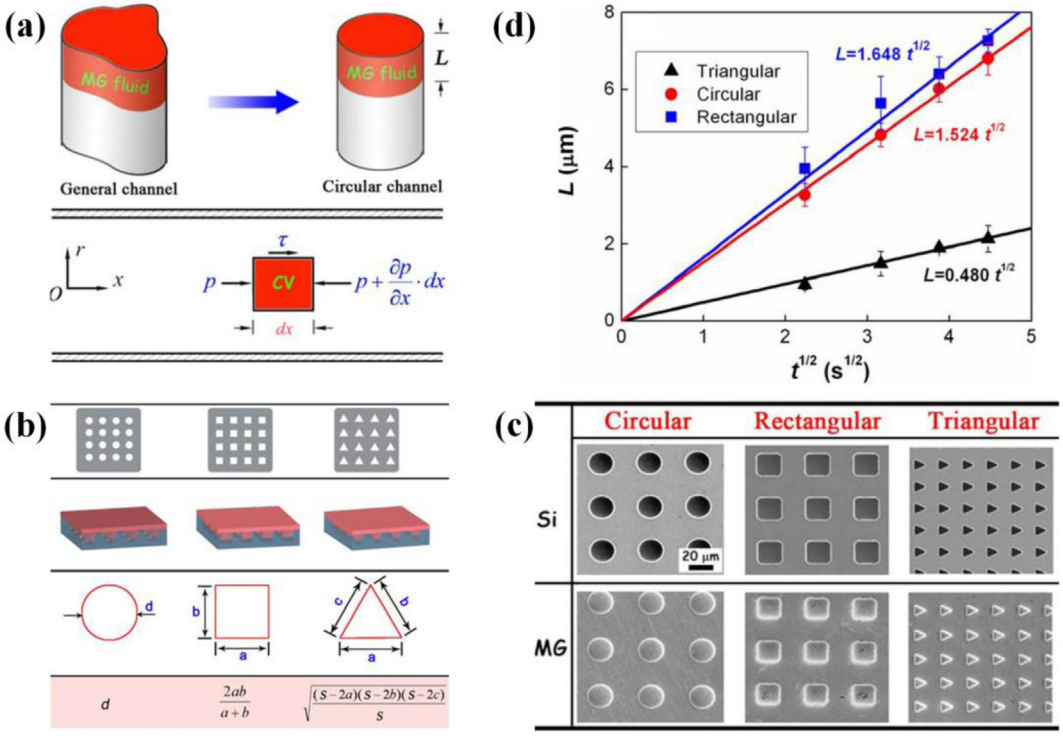

Fig. 2. (a) The equivalence of the irregular channel for MG liquid filling and force analysis of the control volume. (b) Three different microstructures of Si molds for TPF and the corresponding calculation equation for equivalent diameter. (c) Scanning electron microscopy (SEM) images of three different silicon molds and corresponding thermal formed MG samples. (d) The plot of filling length for triangular, circular, and rectangular molds and the solid line is the fit line (Reproduced from Ref. [46]).

Since the mold filling state directly determines the forming fidelity, great efforts have been made to explore the mold filling process in the TPF of BMGs, such as the filling kinetics, interfacial friction and capillary force, etc. The filling kinetics of BMGs in SCLR has been generally studied focusing on regular cylindrical molds [45], while most of the mold cavities in practical forming are irregular shapes. A more universal kinetic equation is established to describe the microfilling process of MG supercooled liquid in the mold with different cross section shapes [46], as shown in Fig. 2a, the hydraulic equivalent diameter based on fluid mechanics was proposed to transfer the mold channel with irregular cross section to a circular one, thus, according to the filling kinetic analysis, the mathematical relations can be obtained between filling length and the processing factors including applied pressure, forming time, liquid viscosity and channel equivalent diameter. A series of TPF experiments of Pd-based BMGs have been conducted using Si molds with different cross sections such as circular, rectangular, and triangular ones (Fig. 2b), the MG replicas fit the Si molds well within variation less than 1% (Fig. 2c) and the experimental data of filling length are consistent with the theoretical values calculated from the proposed model (Fig. 2d), indicating that the universal kinetic equation can be used to design the miniature fabrication processes of BMGs in TPF.

In the forming of smaller scale or high aspect ratio structures, the interfacial friction and capillary force become more pronounced between the metal liquid and molds. Micro-extrusion tests revealed that better mold filling ability of MGs liquid can be obtained at the Newtonian flow regime with the adhesion mechanism of interfacial friction rather than the non-Newtonian with the furrow behavior [47]. In addition, it is suggested that the supercooled MGs liquid should partially wet the molds to facilitate the controllable and precise structures forming under proper stress [48]. In order to reduce the capillary force and resistance to flow during TPF, the strategies such as selecting the matched mold material for the specific MGs [37] or introducing an oil layer to the interface [49] have been carried out to regulate the wetting behavior between the MGs liquid and mold. To give a systematic guidance for the TPF, several evaluation factors have been put forward considering the thermal stability and thermoplastic formability of BMGs with different compositions, such as filled proportion in V-grooves (Rf) [50], SCLR range (ΔTx) [36], fragility correlated with intrinsic viscosity (m) [51], and the maximum diameter of disc fabricated by TPF (d) [23]. Based on in-depth understanding of forming mechanisms of BMGs in SCLR, a lot of TPF approaches have been developed to synthesize various structures ranging from nanometers to centimeters for diverse applications.

2.2. Joining of bulk metallic glasses

BMGs have wide potential applications in advanced fields, due to the excellent mechanical properties and unique material functions. However, a fast cooling rate and sufficient glass forming ability (GFA) are essential to obtain amorphous structure, which limits the maximum size of the as-cast BMGs; for example, the largest critical size of the monolithic BMGs fabricated so far is 80 mm [7]. These issues have greatly hindered the materials engineering applications. Therefore, joining BMGs to get rid of the casting size limitation is presently attracting immense research interest. A variety of joining methods have been developed to achieve the interface metallurgical bonding of BMGs, such as spark welding [52], electron beam welding [53], laser welding [54], explosive joining [55], and the BMGs have been successfully welded to BMGs or crystalline metals. While, based on these methods, BMGs samples were joined in the liquid phase above the melting point, which needed a subsequent rapid cooling process to retain the amorphous structure. Thus, the crystallization of the weld bead and heat-affected zone is difficult to avoid especially for the BMGs with ordinary thermal stability, and the microcracks that may occur in the bonding interface due to volume contraction are also detrimental to the material performance of joined workpiece [56].

Joining of BMGs in supercooled liquid phase by TPF has been proved a promising solution to form a strong metallurgical bond on the joined interface. That aims to achieve diffusion bonding of the superplastic Newtonian flow in SCLR under relatively low temperatures. Friction welding method has been performed on BMGs to locally heat the interface materials to SCLR by high-pressure friction and join the samples together [57]. Though the protrusions will be generally formed around the paired interface by samples deformation, the full contact and bond of the interface free from pores and cracks can be attained due to the superplastic viscous flow of BMGs. Friction welding has been successfully carried out to join BMGs with the ones containing similar and dissimilar compositions [58]. Under well designed conditions, no visible boundaries or defects were observed on the bonding interface, and the joining strength of the welded BMGs without crystallization was found to be the same as that of the previous BMGs or more [59,60]. The process before onset of friction was suggested to be conducted before performing friction welding to break the oxide film and improve the bonding quality [61]. However, the temperature distributed on the samples interface during friction welding process is difficult to control for specific BMGs. Numerical simulation and experiments show that the highest temperature appears on the edge of friction interface while the lowest temperature is in the center [62], indicating that the edge temperature needs to be carefully regulated below the crystallization temperature Tx. An equation considering the thermal effect on amorphous structure was established for selecting the critical friction time for friction welding of BMGs.

Another feasible joining method based on TPF is to heat and bond the BMG specimens while keeping the interface relative still. Based on the superplastic flow theory, the diffusion bonding model for Zr-based BMGs in SCLR was developed to calculate the optimal bonding time reducing the interface voids at a certain bonding temperature [63]. However, the compression tests of the bonded BMGs also found incomplete joining, maybe due to lack of grain boundaries acting as bypasses to transport atoms to vanish the original voids on bonding interface [64]. To improve the thermolplastic joining quality of BMGs, the influences of temperature and pressure on diffusion behavior along with time have been generally studied. During thermolplastic bonding of BMGs, it has been found that the micropores on the bonding interface gradually shrink to nanovoids and diffuse outside the sample under certain TPF parameters, forming atom-to-atom bonding across the interface [65]. The high bonding temperature and long bonding time facilitate diffusion to achieve better metallurgical bonding, while the diffusion tends to induce structural relaxation of BMGs leading to brittleness inside the joined specimens. An effective solution for this issue has been proposed by using a relatively low bonding temperature and short holding time [66], as shown in Fig. 3a, multilayer Pd-based BMG sheets were stacked together and heated to the bonding temperature at a heating rate of 60 K/min by applying electric current to the samples under a vacuum environment, and the bonding parameters were elaborately estimated and selected based on the TTT curve of the specific BMGs, for instance, the bonding temperature was adopted as only 10°K–20°K higher than Tg to minimize the structural relaxation and the corresponding holding time was also determined according to the time-temperature-transformation (TTT) curve to avoid crystallization. Compression tests prove that the fracture strength and plasticity of the multilayer bonded samples were significantly improved

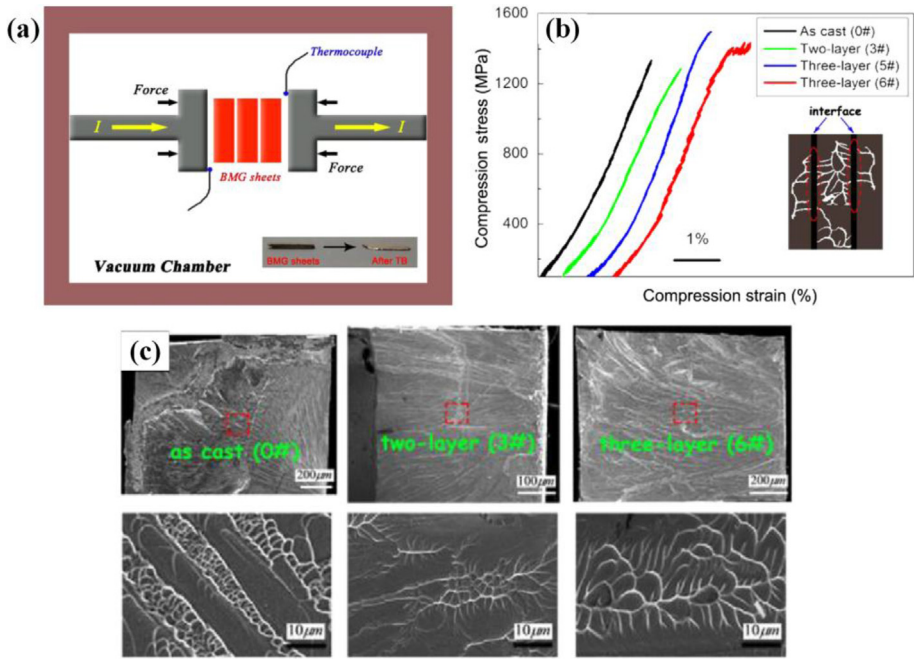

Fig. 3. (a) The principle of thermolplastic bonding of multilayer BMGs. (b) Compression stress and strain curves of the as cast, two-layer (3#) and three-layer (6#) BMGs. (c) The fracture morphologies of the as cast (0#), two-layer (3#) and three-layer (6#) BMGs (Reproduced from Ref. [66]).

(Fig. 3b), and the three layer bonded specimen tended to achieve a more significant plasticity enhancement than that of the specimen, because the latter underwent a longer bonding time leading to its brittleness. The radiating ridge patterns were observed on the fracture surface of the bonded BMGs in contrast to the river-like fracture morphology of the as-cast sample (Fig. 3c), indicating that the improvement of plasticity is due to the blocking effect of the multilayer bonding interfaces on the propagation of shear bands.

Besides, the oxidation films existing on the BMGs interface are also generally concerned in the thermolplastic bonding, because they act as barriers to the contact and diffusion of metal atoms. The TPF of BMGs to obtain atomically smooth surface demonstrated that the surface oxidation can be remove out of the forming area by the lateral flow of the supercooled liquid [67], indicating the possibility of BMGs joining using this method. Whereafter, the joining of BMGs with oxidation films in air has been successfully achieved on a timescale of milliseconds to seconds at low pressure and temperature [68], though some oxidation debris still existed in the bonded interface. The bonding mechanisms were proposed that the superplastic flow of BMGs breaks the surface oxidation films and thus the pristine alloy flow towards the interface to contact and form the metallurgical bonding. A prediction model for the bonding strength was developed based on the original material properties and bonding stress. Based on the joining experiments and finite element method (FEM) simulation, the joint strength of BMGs has been found solely determined by the area fraction of the bonded regions, and the bonded regions increase with the joining temperature and time [69], providing guidance for process optimization. A high-speed heating strategy with a rate of 2000 K/min has also been developed to improve the joining quality in thermolplastic bonding [70]. The high heating rate of BMGs taking microseconds to milliseconds to reach the SCLR can drastically decrease the viscosity of the supercooled liquid to a low magnitude such as 10^3 Pas for the Zr-based BMGs, which is of benefit to filling cavities on the interface and forming strong metallurgical bond even at very low pressure such as 0.1 MPa. The general equation involving the viscosity of supercooled liquid and the thickness of the surface oxidation film was established to determine the optimal bonding timescale for BMGs in high-speed heating-associated bonding. Although the bonding mechanisms still need further studies, the joining processes of BMGs based on TPF are promising to synthesize larger BMGs and scale up the cellular structures [71].

2.3. Fabrication of micro-/nanostructures

BMGs have attracted extensive interest to be a versatile platform for miniature fabrication for the structural and functional applications. Due to the superplasticity and small solidification shrinkage in SCLR [36], a variety of micro-/nano surface structures or three-dimensional (3D) parts of BMGs have been obtained by TPF with high fidelity. Microchannels are the essential patterns for microfluidic systems to precisely control the flow of trace amounts of liquids or gases, which is promising to have application in the high throughput detection and analysis in biological and medical sciences. Researches, both theoretical and experimental, have been done to fabricate these patterns on BMGs by TPF that were previously unachievable with conventional crystalline metal processing. Hot embossing has been conducted on Zr-based BMGs using a silicon master mold to obtain the channels (50 μm in width) with single and continuous bends featuring structure [72]. Despite the significant difference in thermal expansion coefficients, the seamless interface between the BMGs and silicon mold was observed in the forming simulation and TPF process, and the maximum filling length of the supercooled liquid exhibiting laminar flow during TPF can be predicted and tuned under certain process parameters, ensuring the replication accuracy of the BMGs microchannels. It is suggested that to improve the integrity of the formed channels, the Newtonian flow behavior of the supercooled BMGs during TPF need to be achieved by regulating process parameters based the established TPF map [44]. A hybrid microchannel including the features of angles, circular arcs and intersections has been synthesized on the Pd-based BMGs by TPF [73], as shown in Fig. 4a, these patterns are generally regarded as important indexes to evaluate the

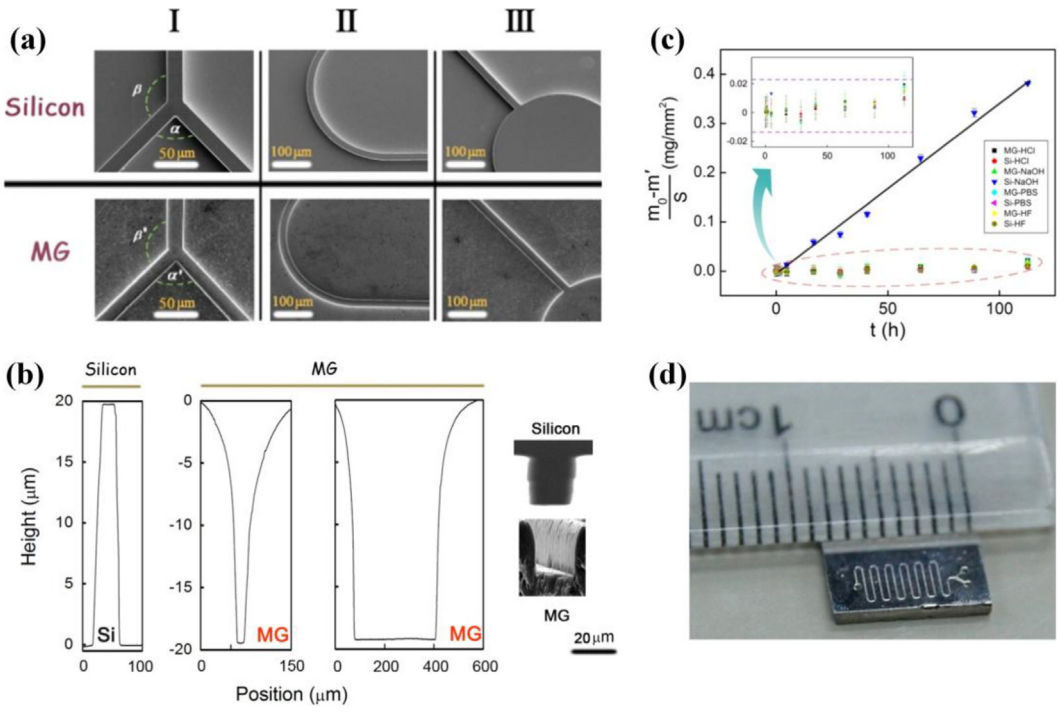

Fig. 4. (a) SEM images of silicon mold and BMG microchannels at concerned areas I, II and III. (b) The height of the microstructure on silicon mold and the corresponding depth of BMG channels at different positions. (c) Mass loss of silicon and MG per unit area in different corrosion solutions with the increase of time. (d) Photograph of the formed BMG microchannels (Reproduced from Ref. [73]).

forming quality of microchannels, due to the formability decline induced by geometry changes. The width of the formed grooves was 18.45 ± 0.05 μm with only a slight average error of about 0.27% compared with the silicon mold, the variations between the formed angles and the designed ones in area I are less than 0.1°, and the depth of the BMG channels in different areas are very close (Fig. 4b), indicating that high dimensional accuracy and good uniformity of the channel patterns have been achieved by the TPF process. The subsequent corrosion tests as shown in Fig. 4c verified the excellent corrosion resistance of the channels in the acid and alkali solutions, demonstrating that the formed BMGs structures (Fig. 4d) are very favorable for the microfluidic systems used in different corrosive environments.

The fabrication of micro-/nano-arrays on BMGs by TPF are also generally carried out to obtain the structural surfaces with functions like photoelectricity, catalysis, hydrophobicity, etc. The optical gratings with 600 and 1500 nm periods have been imprinted on the Pd-based BMGs in air by TPF [74]. It is noted that the BMG grating stripes appeared quite smooth after TPF and the polishing marks on the original surface were almost invisible due to the superplastic flow of the BMGs in SCLR. Though the periodicity of grating was faithfully preserved on the BMGs, the replication quality of the 600 nm gratings was not as good as that of 1500 nm gratings, and the corresponding filling length was only about 70% in the mold, because of the increasing capillary resistance force during the smaller scale forming. Despite the residual forming defects, the nano-imprinted BMG gratings showed good color spectra and diffraction properties, while the grating area less than 600 × 600 μm^2 was too small for practical use. The optical gratings with a much larger area of 8 × 8 mm^2 have been obtained by hot embossing within the processing time less than 30 s [75], as shown in Fig. 5, the width of the formed BMG grating ridges and hollows reached 3.5 μm and 4.4 μm respectively, and the filling depth can be regulated by adjusting the forming pressure. It was also found that the flow of metal liquid during filling was delayed on the side wall of mold grooves due to friction force, thus forming a curved shape on the top of the gratings in contrast to the flat top of the mold. (Fig. 5e and f). Nevertheless, the formed BMGs gratings attained the ultrasmooth surface with a slight shrinkage of 1.25%, ensuring more brilliance and better diffraction efficiency than that of the Si master mold (Fig. 5g and h). Besides, due to the high replication fidelity and surface quality, the patterned BMGs with remarkable mechanical properties can be subsequently utilized as a durable mold for the TPF of polymers [74,76,77] and even the BMGs with a lower *Tg* than the BMG mold [48].

The nanowire arrays of BMGs have been extensively fabricated by TPF and applied in biosensing [78,79], energy conversion [80,81] and catalysis [82,83]. The smaller diameter and higher aspect ratio of the micro-/nanowires formed on BMGs are the main research focuses to enhance their performances. One of the difficulties for nanowires formation is the dramatically increased forming pressure due to the significant capillary resistance. According to the aforementioned process optimization in TPF, the nanowires with the minimum diameter of 13 nm and aspect ratio exceeding 50 were synthesized on platinum (Pt)-based BMGs [48], indicating that a wide size range of BMG nanowires can be fabricated. Various surface structures have been patterned on BMGs by TPF to enhance different functions such as the surface wettability. The hierarchically structured surfaces of palladium (Pd)-based BMGs were prepared by two steps to form nano- and micropatterns in sequence [84], as shown in Fig. 6a, the nanopillars with a mean diameter of 80–100 nm was first formed by anodic aluminum oxide (AAO) template and then the periodic micropores were superposed on the nanopatterned surface by a silicon mold. The obtained hierarchical structures consisting of nanoscale protrusions on the microscale textures with well-defined geometries tend to be superhydrophobic (Fig. 6c) while the polished surface is hydrophilic (Fig. 6b). In addition, other sophisticated BMG structures

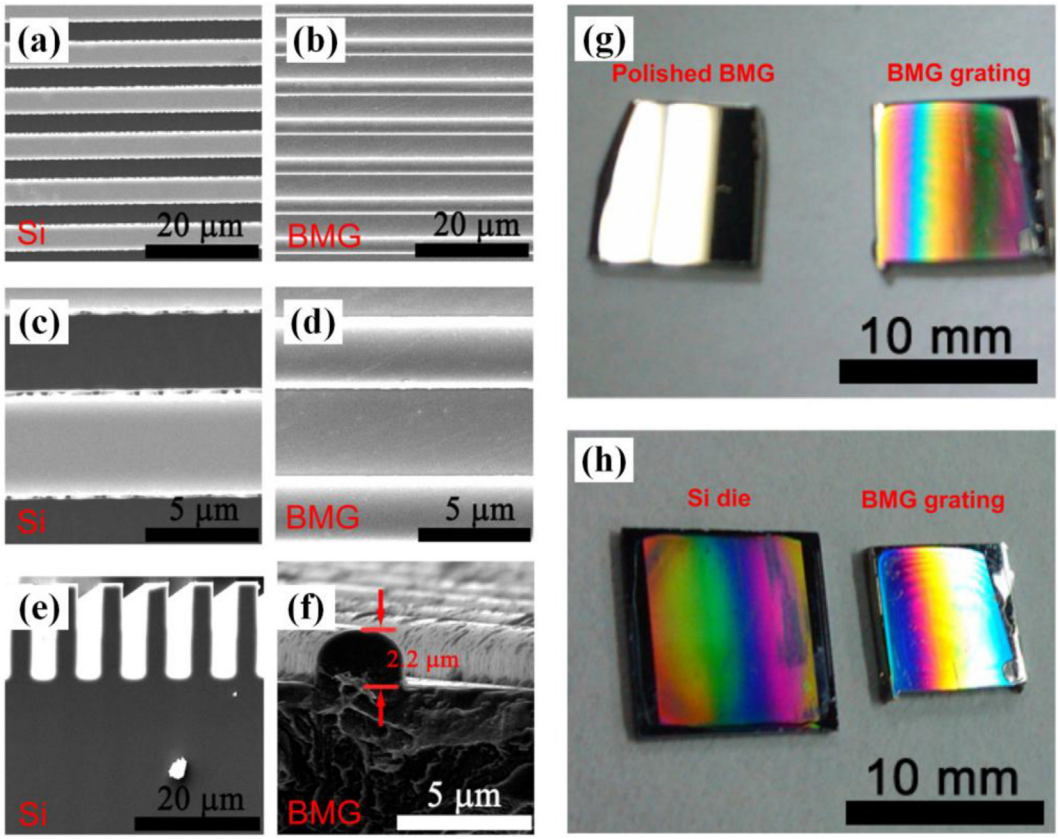

Fig. 5. (a)–(f) SEM photographs of Si die and hot embossed BMG grating, (a) and (b) are the top views, (e) and (f) are the side views, (c) and (d) are the close-up views of (a) and (b), respectively. (g) The polished BMG plate (left) and BMG grating (right) under the shine of fluorescent lamp light. (h) The Si mold (left) and BMG grating (right) under the shine of fluorescent lamp light (Reproduced from Ref. [75]).

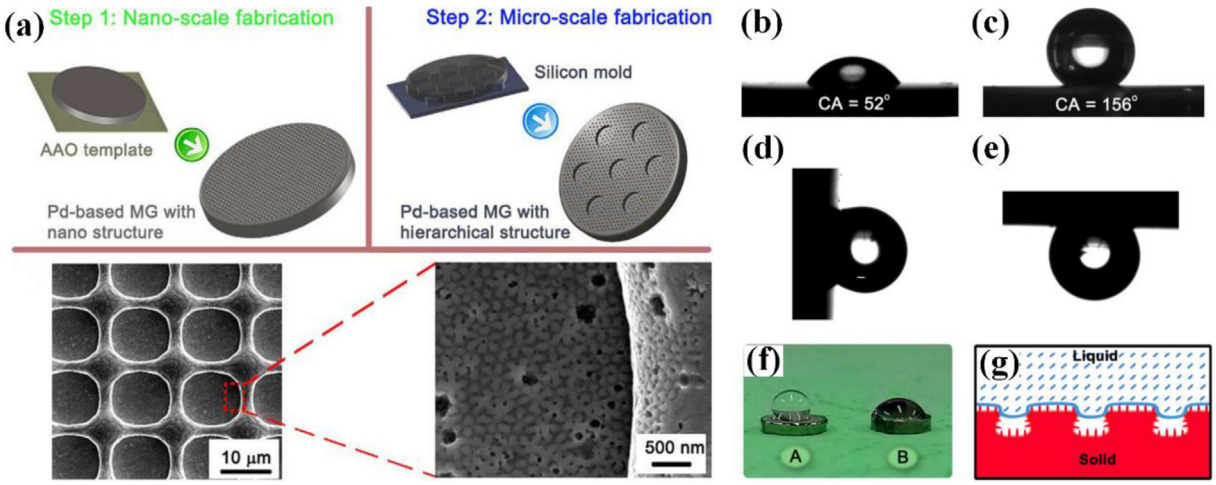

Fig. 6. (a) Fabrication of hierarchical structures on Pd-based BMG by multistep TPF. (b) (c) The water contact angle (WCA) of polished surface and hierarchically patterned surface, respectively. (d) (e) The water adhesion of patterned surface. (f) Wettability of two different surfaces, A: the patterned surface and B: the polished one. (g) The wetting regime (Reproduced from Refs. [84]).

have also been developed, such as the hierarchical surface with hybrid wettability [85], thermolplastic drawing nanowires [86] and the Janus structures with distinct materials [87], demonstrating that the thermal forming approaches based on the superplasticity of BMGs in SCLR can provide a versatile toolbox for the micro-/nanostructures fabrication. However, the thermal effect induced oxidation [24] and chemical segregation [25] of the BMGs structures still need further studies in TPF processes.

3. Ultrasonic-assisted forming

3.1. Plastic behavior under high frequency vibration

In general, vibrations with frequencies above 20 kHz are referred to as ultrasonic vibrations. In 1955, Blaha et al. [88,89] found that the metal materials undergo a significant softening phenomenon accompanied with reduced strength under ultrasonic vibration, which is called the Blaha effect. Based on these characteristics, the ultrasonic vibration-assisted forming technology had been developed, which is widely used in various plastic processing processes. Hung et al. [90] studied the mechanisms of the deformation resistance reducing of A6061-T6 aluminum alloy during compression assisted by ultrasonic vibration, finding that the temperature of the sample during compression under the loading of ultrasonic vibration is higher than that of traditional compression and the increase of sample temperature and the absorption of vibration energy by dislocations are beneficial to lower the deformation resistance of metal. Jimma et al. [91] studied the effect of ultrasonic vibration on the microdrawing of foils. It was found ultrasonic vibration can significantly reduce the punching load and friction during the forming process, and ultimately increase the tensile ratio of the material. Takemasu et al. [92] studied the effect of ultrasonic assistance on micropunching, showing that the ultrasonic vibration can suppress the generation and expansion of cracks and make the tear zone area smaller, which is of benefit to improve the quality of shear punching. In addition, the ultrasonic vibration-assisted processing technology is also applied to extrusion [93], forging [94,95], wire drawing [96], electric discharge machining [97], etc. These research works demonstrate that the ultrasonic vibration assistance plays a significant role in promoting the plastic processing of metallic materials.

Metallic glass (MG), also known as amorphous alloy, is a new type of multicomponent alloy with excellent mechanical and physical properties [98]. However, the inherent brittleness acting as Achilles' heel of MGs has been one of the major obstacles that hinder its wider application [99]. To find suitable solutions for the above problem, researches in recent years have combined ultrasonic vibration assistance with amorphous alloys' forming. Li et al. [100] and Han et al. [101] introduced ultrasonic vibration in the thermoplastic forming of zirconium (Zr)-based MGs, and found that the high frequency vibration assistance can significantly improve the formability of MGs; in addition, the thermal formability is positively correlated with the ultrasonic amplitude. Lou et al. [102,103] proposes an ultrasonic vibration-assisted compression technique for MGs, finding that MGs can achieve rapid structural rejuvenation under the exertion of ultrasonic vibration, and become more heterogeneous with better plastic deformation ability after the ultrasonic vibration loading. Besides, plastic strain occurred in the fracture surface of MGs during ultrasonic compression, indicating that as the ultrasonic amplitude gradually increases, the yield strength of the alloy decreases and the ductility is enhanced, which can significantly improve the formability of MGs at room temperature.

3.2. Shear punching assisted by ultrasonic vibration

In terms of plastic processing of MGs, an energy-efficient punching method has been proposed as ultrasonic vibration-assisted shear punching (USP) [35,104,105]. The schematic diagram of USP is depicted in Fig. 6, an ultrasonic punch with a fixed 20 kHz vibration frequency and adjustable main pressure was placed at the top, the ultrasonic punch was made of cemented carbide (TC4 titanium alloy in present work) with a tip diameter of 5 mm. And then, a pressure plate with a stock bin was placed under the punch, the diameter of the stock bin was 5.1 mm. Under the pressing plate, the workpiece and mold were placed in turn. All the components were centered and this combined shear punching device can be used not only for microscale MGs strips but also for macroscale BMGs.

When USP was applied to MG strips, ethylene vinyl acetate (EVA) plastic powders with an average diameter of 300 μm was put into the stock bin (Fig. 7a). Once the punch drops, the severe friction caused by ultrasound would quickly heat the EVA plastic powder into a molten state, which can transfer pressure and vibration to the MG workpiece. Finally, the MG ribbon would be punched with holes under the dual effects of pressure and ultrasonic vibration. The introduction of molten plastic between the punch and MG ribbon instead of the rigid punch has unique advantages, which can serve as a medium for transmitting pressure and vibration to the MG workpiece (Fig. 7b), and the anisotropic holes with complex contours can be obtained rather than simple round hole. As shown in Fig. 8(a–i), this plastic forming process by USP has been extended to a variety of typical MG ribbons and structures, including $La_{55}Al_{25}Ni_5Cu_{10}Co_5$, $Al_{86}Ni_9La_5$, $La_{60}Al_{20}Ni_{20}$, $Fe_{78}Si_9B_{13}$ and $Cu_{50}Zr_{50}$, demonstrating the universal applicability of the USP method to MGs. When USP is performed on the thicker BMG plate, flexible punching for the MG ribbons are no longer applicable due to insufficient strength, and the rigid punching must be adopted to achieve effective forming (Fig. 7c). However, the hole parts obtained through the rigid punching can only be simple round holes matching to the cross-section shape of the punch. It is worth mentioning that under the exertion of ultrasonic vibration, the Zr-based BMG workpiece with a thickness of 1 mm can be punched out extremely quickly (less than 1 s) with perfect quality, as shown in Fig. 8(j and k); the USP stress for the BMGs that needs to be provided is 110 MPa, only one-tenth of the theoretical stress based on the conventional punching method. However, it was also found that those crystalline alloys that are lower in strength and seem to be more easily formed than MGs failed to be punched out by utilizing the same USP method, indicating that MGs and crystalline metals follow different deformation mechanisms under the high frequency ultrasonic vibration.

Researchers attribute the low-stress forming of MGs at ambient temperature to the evolution of the unique amorphous atomic structure under ultrasonic vibration [35,106,107]. The structure of MGs is considered to be a combination of elastic matrix and dispersed sites. Due to such unique structures, the specific liquid-like regions can couple with the high-frequency hammering and absorb the hammering energy, resulting in the activation of α-relaxation of MGs when the hammering progressed. As illustrated in Fig. 9a, during the forming process, the central part of the MG plate was suspended and the part along the edge of the mold is restricted. Thus, when the ultrasonic vibration is transmitted to the MG workpiece, the energy absorbed by the center part of the MG plate can be dissipated by its own elastic vibration, but the energy absorbed by the edge part will be stored continuously. When the energy stored in the confined area of MG plate reaches a certain threshold, the liquid-like region inside the MG will be activated to couple with the surrounding elastic matrix, eventually causing the local softening of the MG plate. The magnified illustration in Fig. 9a reveals the microprocess, and the soft region of the MG plate from top view was schematically drawn. The USP of BMG plate has been successfully carried out and a phenomenological model of cyclic liquefaction of the amorphous atomic structure was proposed to understand the underlying mechanism of USP (Fig. 9b). In the proposed model, the special interior structure of MGs is analogized to the soil in nature. The liquid region and elastic matrix in MGs are similar to solid soil and liquid water in saturated or partially saturated soil, the cyclic loading of stress would result in loss of stiffness

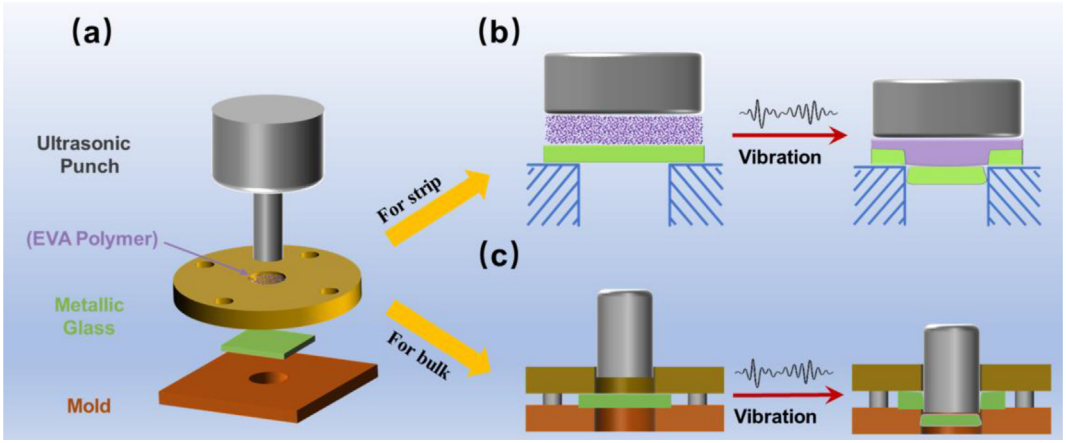

Fig. 7. (a) Illustration of the combined devices of ultrasonic vibration-assisted shear punching (USP). (b) The forming process of MG strips during USP. (c) The forming process of BMG plate during USP (Reproduced from Ref. [35,104]).

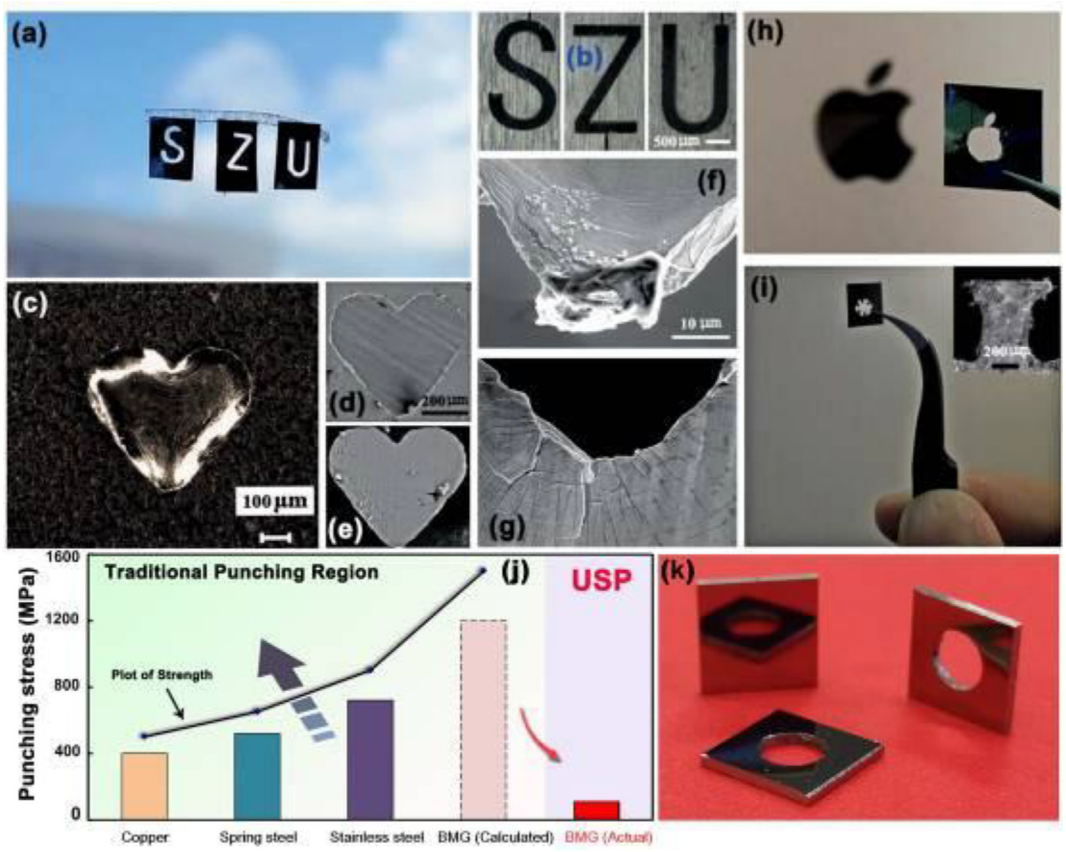

Fig. 8. (a) The photos of MG ribbons after punching out the capital letters 'S', 'Z' and 'U'; (b) The stereomicroscope images of the letter molds; (c) The optical microscope image of the heart-shaped product; (d) (e) The SEM images of the MG ribbon with a heart hole and the paired product; (f) (g) The magnified images of (d and e); (h) A macroscale punched Apple's logo compared with the real logo on iPhone 6 (Reproduced from Ref. [104]). (i) A typical stator core fabricated by the USP method in 0.05 s. (j) The variation of punching stress for MGs and crystalline metals under UPS and conventional punching. (k) The shear punched Zr-based BMGs with a thickness of 1 mm and a diameter of 5 mm. (Reproduced from Ref. [35]).

and strength of saturated soil [108,109]. In the present work, ultrasonic vibration as a typical cyclic load will cause similar effects on amorphous alloys. Under the action of ultrasonic vibration, the liquid-like regions in MGs can be activated and extended, causing the increase of their fraction. When enough liquid-like regions are activated and connected, the interconnected elastomer network will be destroyed, and the strength and stiffness of the MG will be reduced, which is more conducive to forming the MGs.

In addition, the application of ultrasonic vibration assistance has been also extended to the forming of MGs by template. By introducing ultrasonic vibration to the interface between the sample and mold, a novel forming route for BMGs was proposed [110],

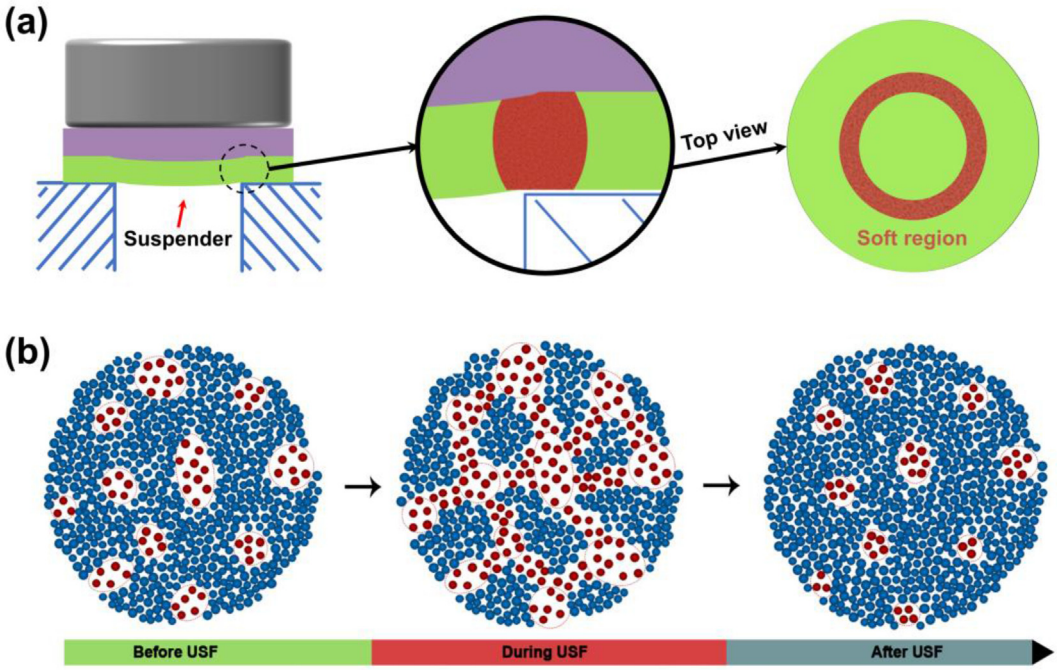

Fig. 9. (a) The details of the MG plate around the mold edge and the soft region of the MG strips from top view during the ultrasonic hammering. (b) The schematic diagram of cyclic liquefaction in MG during USP process (Reproduced from Refs. [35,104,105]).

which is named ultrasonic beating forming (UBF). As shown in Fig. 10 (a,b), the BMG sample was repeatedly beaten 20,000 times per second under certain pressure force by a cylinder ultrasonic indenter within a very short period of time, causing the BMG sample to get hot and soft, resulting in thermoplastic forming. During the UBF, heating and forming are completed simultaneously in less than 0.5s, which avoids the risk of the BMGs being oxidized and crystallized during the forming process. A series of MG structures ranging from macroscale to nanoscale can be obtained by UBF in a very short time, as shown in Fig. 10(c–j): the Zr-based MGs were effectively squeezed into different geometric shapes of macromold cavities retaining the original metallic luster, and the distinct micro/nano patterns have also been obtained on the MG surface, demonstrating that UBF is feasible for the precise structures fabrication of MGs while avoiding the crystallization and oxidation.

3.3. Ultrasonic manufacturing

Ultrasonic manufacturing has also been conducted to bond the small-size MGs to form large workpiece, which can break the limitation of glass forming ability (GFA) on the size of as-cast MGs. At present, various welding methods have been applied to the manufacturing of MGs, such as laser welding [111], electron beam welding [112], arc welding [113], resistance spot welding [114], reactive foils welding [115], and explosive welding [116]; these welding methods with very high instantaneous welding power and short duration can be seen as liquid phase welding for MGs, which can reduce the thickness of heat-affected zone (HAZ) to avoid devitrification. However, these methods have the defect that the interface of the joint MGs is not completely amorphous, because it generally needs to be heated beyond the crystallization point (T_x), or the reaction time is too long to make the part of the joint crystallize. Another kind of supercooled liquid-phase welding, which forms the joint based on the superplasticity of MGs in SCLR, has now been developed as ultrasonic welding [117] and friction welding [118]. This welding method is to control the temperature of MGs within its SCLR by adjusting the process parameters and simultaneously exerting a certain pressure to complete the mutual bonding of the paired samples by superplastic flow and deformation. The ultrasonic vibration has been considered as an effective route of energy input in the bonding interface with the advantages of low energy loss, simple operation, environmental protection, etc. [119] It was proved by experiments that the effect of ultrasonic energy on the softening process of metal is equal to the heat energy of the order of 10^7 [120], which is favorable for the bonding of MGs. Conventional ultrasonic welding processes can be divided into two categories, as shown in Fig. 11, one is called ultrasonic metal welding (UMW) with the vibration direction paralleling the welding interface, which is generally used for metal welding at a vibration frequency higher than 15 kHz; the other one is ultrasonic plastic welding (UPW) with the vibration direction perpendicular to the welding surface.

As early as 1978, UMW method had been carried out to bond Fe-based MG ribbons with copper with no crystallization in the welding interface verified by the transmission electron microscopy (TEM) test [121]. It is the first application of ultrasonic welding in MGs, starting the exploration of the combination of MGs welding and ultrasonic processing technology. In 1983, UMW was also found suitable to weld Ni-based and Fe-based MG ribbons to the crystalline metal such as aluminum [122]. But in the following decades, the ultrasonic welding technology for MGs has no significant progress. Until 2007, the UMW was considered to be effective for the bonding between MG samples that could weld two 50 μm thick strips of $Zr_{55}Cu_{30}Ni_5Al_{10}$ MG with or without external heat [123], extending the ultrasonic welding process to the bonding between MGs. And in further work, it was clarified that under the action of ultrasonic vibration, the interface of MGs formed a certain amount of bonding area without crystallization, and the highest temperature (676 K) in the process of UWM was just above the T_g of MGs, and the total time exceeding T_g during bonding is rather short [124], which effectively reduced the risk of crystallization. A

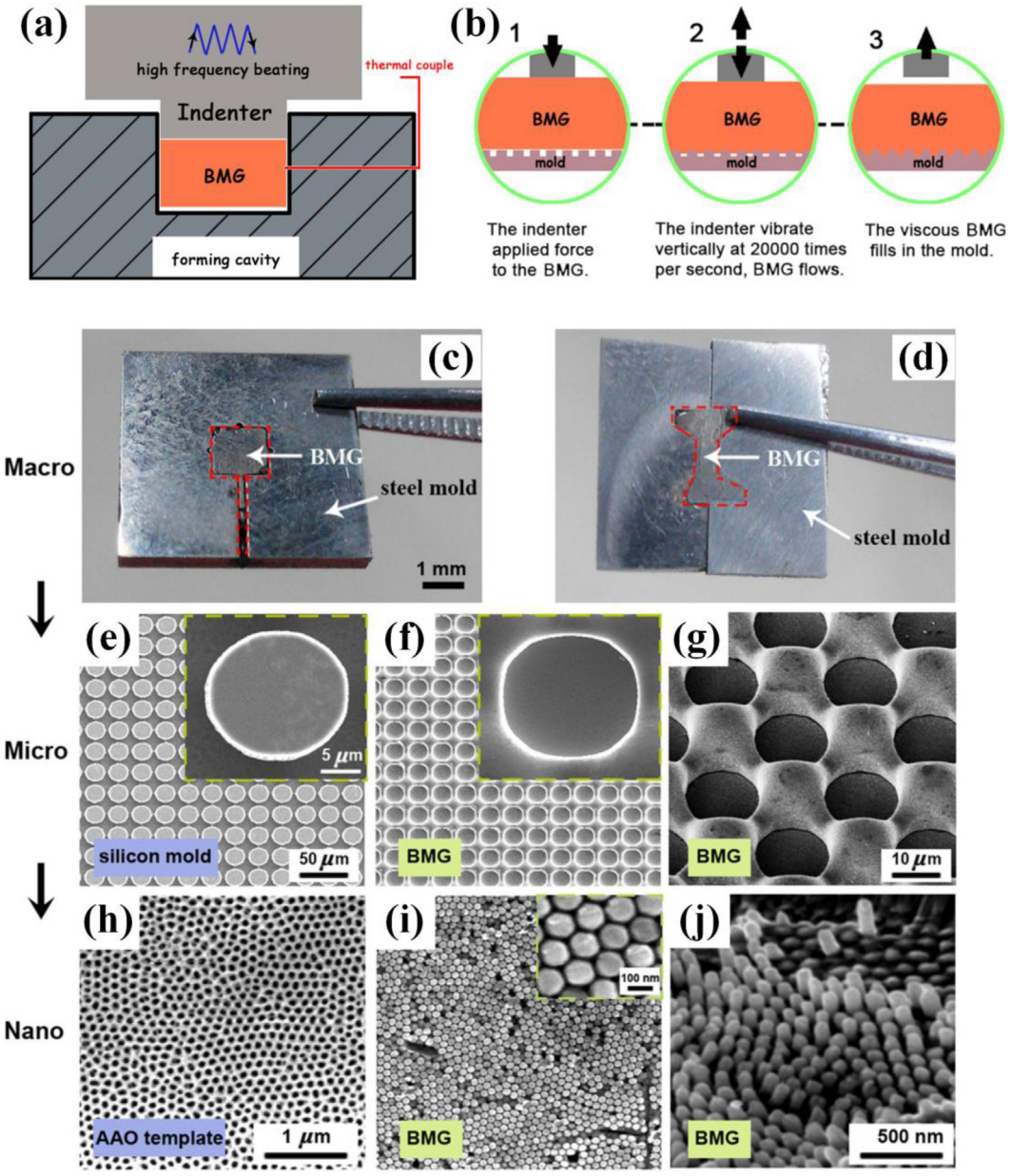

Fig. 10. (a) Schematic diagram of the ultrasonic beating forming (UBF) setup. (b) Illustration of the UBF process in molds. (c,d) BMGs fill into macro rectangular hole and the dog-bone shaped hole. (e), (f,g) SEM images of the silicon molds and corresponding microstructures after UBF. (h), (i,j) The nanoscale morphology of the AAO template and the as-fabricated BMG surface (Reproduced from Ref. [110]).

schematic time-temperature-transformation (TTT) diagram has been established to illustrate the relationship between the devitrification criteria and the thermal history applied to MGs by casting and welding respectively, as shown in Fig. 12a, indicating that MG strips can also be bonded to each other to form fully amorphous joints by ultrasonic welding at a relatively low temperature. Then, the 1 mm thick Cu-based BMG samples were successfully welded without crystallization and external heat by UPW [117], demonstrating the great potential of ultrasonic welding technology in the manufacturing of large-size MGs.

In-depth research has been conducted on how ultrasonic vibration works in the soldering of BMGs. A 40 kHz ultrasonic wave was applied on the tin (Sn)-based alloy used as solder and zirconium (Zr)-based BMG as substrate, finding that the role of ultrasonic vibration is not only to raise the temperature, but also to remove the passivated film and roughening surface on BMG by ultrasonic cavitation. Meanwhile, the capillary effect of ultrasonic cavitation can also enhance the flow ability of MGs in the welding interface, inducing the anchoring effect to forming the welded joints [125]. This beneficial effect then was also found in the copper (Cu)-based BMG under the action of ultrasonic vibration, confirming the universality of anchoring effect in the ultrasonic welding of MGs [126]. However, the bonding of MGs can not only rely on the mechanical adhesion brought by anchoring effect, due to the low tensile strength of the bonded MG obtained in this way. Therefore, a more effective welding process by using the bonding effect of intermetallic compounds (IMC) was developed based on ultrasonic welding. Ji et al. used UPW technology to weld Fe-based metallic glass strips to aluminum plates with the help of Sn-based filler and external heating [127]. In this way, not only the anchoring

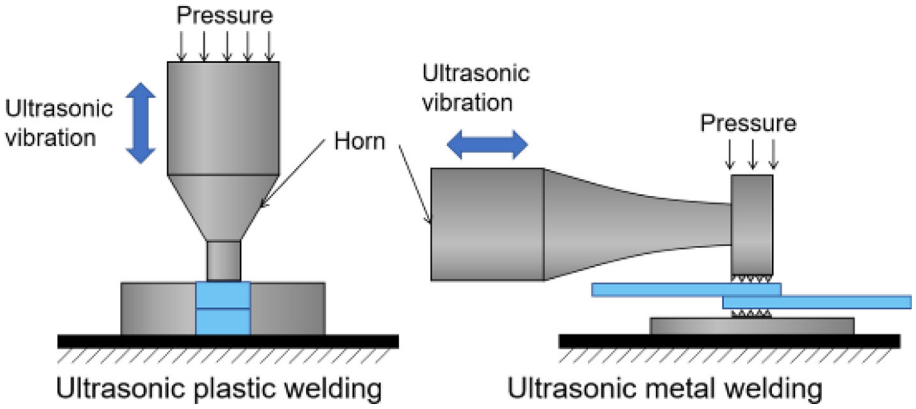

Fig. 11. Schematic diagram of ultrasonic vibration welding.

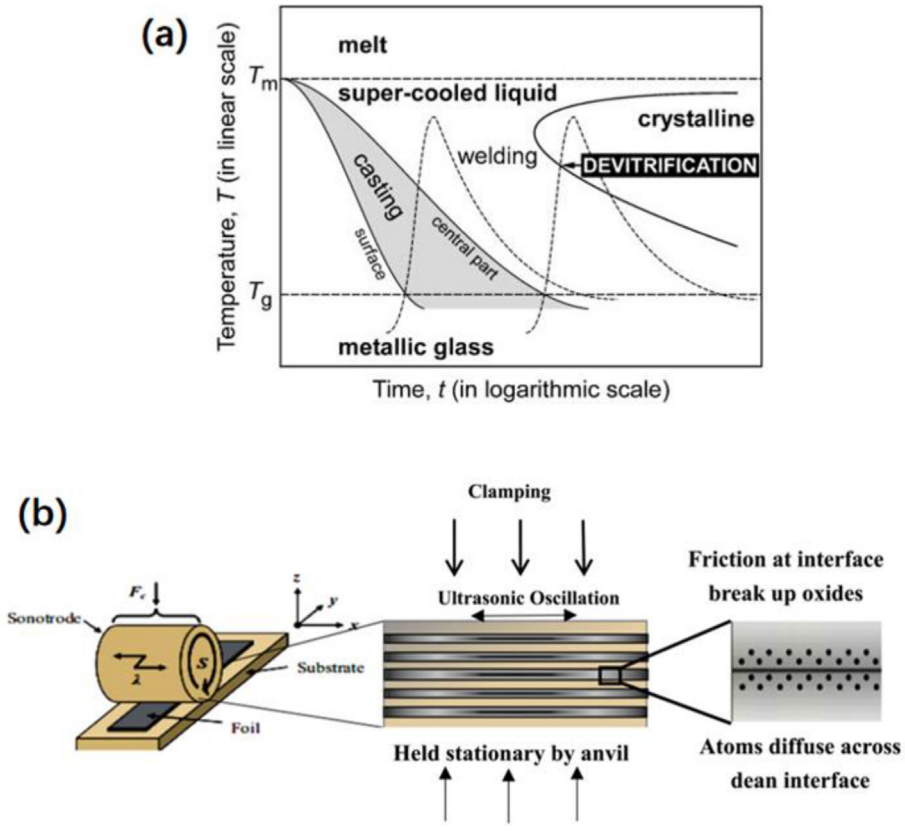

Fig. 12. (a) Schematic of TTT diagram showing the relationship between the devitrification criteria and the thermal history of MGs (Reprinted from Ref. [124]). (b) Schematic diagram of ultrasonic consolidation process in ultrasonic consolidation (Reprinted from Ref. [132]).

effect was achieved, but also the wetting behavior and interface reaction have taken place, resulting in the IMC of $FeZn_{13}$ (intermetallic compound in biodegradable Zn Fe alloy) and nickel aluminide ($NiAl_3$) in the interface to form a robust MG and aluminum joint. Recently, Zhang et al. fabricated Zr-based BMG joints with Zn−3Al hypoeutectic filler metal and external heating through the UPW [128], and a thick $Zn_{50}Al_{25}Zr_{25}/Zn_{22}Zr$ IMC layer was formed on Zr-based BMG substrate surface, bringing a shear strength of about 100 MPa for the bonded samples.

In addition, the method of fabricating multilayer MG strips by ultrasonic welding has also been developed. This method may be used as a ultrasonic manufacturing process like 3D printing that thin metal strips are stacked layer by layer to obtain thicker metal samples. It can be imagined that if the metallic glass strips can be superposed infinitely under the action of ultrasonic vibration, the limitation of GFA on the size of MGs will no longer exist. Song et al. successfully welded multilayer Fe-based MG strips for the first time using UWM technology with a joint area reaching 8 × 8 mm^2 and 4−5 stacked layers (each layer is 25 μm thick) [129]. Similarly, multilayer Ni-based MG strips were also bonded by ultrasonic welding, stacking 3−4 MG layers (each layer is 40 μm thick) [130]. Besides, a composite sample that two Al/Cu crystalline ribbons clamp a Ni-based MG ribbons has also been obtained by UPW process [131]. However, the laminated MGs manufactured in the

above works can be only welded to several layers and the alternate stacking like in 3D printing still cannot be achieved, which need to be further extended to the more versatile manufacturing process. A novel ultrasonic consolidation method has been developed [132], as shown in Fig. 12b, the commercial 1060 aluminum foil and Fe-based MGs were alternately placed under the ultrasonic vibration roller with the heating from bottom, the two kinds of materials gradually produced synergistic plastic flow and deformation under the coupled action of ultrasonic vibration, axial pressure and external heating, and finally the composite joints of aluminum and MGs were formed, and the maximum tensile strength of the fabricated composite sample consisting of tough layers and stiff layers was reaching to 165 MPa which is superior to that of the 1060 aluminum layer (120 MPa).

Recently, three typical MG debris (Zr-, La-, Pd-based) have been successfully bonded to be one sample by UPW, and even the multiphase composite of BMGs was obtained by mixing the different MG debris together, as shown in Fig. 13 (a, d, e), which can be called metallic glass-glass composites (GGCs) [34]. In the previous researches, the mechanisms of ultrasonic welding of MGs are generally considered as anchoring effect, chemical action or mechanical metallurgy, etc. However, a new bonding mechanism has been proposed in this work that the atomic diffusion speed on the surface of MGs is accelerated under the high frequency ultrasonic vibration and then the joint interface can be formed at room temperature. According to Cao et al. the atomic diffusion rate on the MG surface is millions of times faster than that inner surface [133], but just a short contact between the two MG samples will not result in an effective bonding joint, thus the UPW technology was adopted to speed up the bonding of MGs. The molecular dynamics (MD) simulation of $Zr_{50}Cu_{50}$ MG is also carried out to study the change of activation energy of MG surface along with depth, and it is found that the activation energy of the surface is significantly lower than that of its interior, as shown in Fig. 13 (b, c). In order to further understand the surface activation under vibration loading, the dynamic scanning probe microscopy (DSPM) was used to study the surface mobility of MG samples. It has been found that the viscoelastic loss tangent (tanδ) corresponding to the internal friction dramatically increases as the driving frequency increases from 200 to 70,000 Hz, as shown in Fig. 13 (f,g), resulting in viscosity at the surface decreasing to three orders of magnitude. A relatively high internal friction (tanδ = 0.2) was observed in the MG surface layers activated by ultrasonic vibration at a temperature far below *Tg*, which is close to the internal friction generally observed in the MG samples around the *Tg* [134]. These results manifest that the surface atoms in MGs activated by high frequency vibration have very high mobility, inducing rapid bonding of MG interface at ambient temperature and low stress. Based on the above theory, two-phase and three-phase MG composites are obtained with excellent bonding quality and retained amorphous structure. The ultrasonic-assisted forming of MGs provides a new way to fabricate structures and large-size of MGs, possessing great potential in the future development and applications.

4. Summary

In the past decades, significant progress has been made in the fabrication of various structures ranging from nanometers to centimeters based on the plastic forming processes of MGs, such as surface patterns, 3D parts, and large-size BMGs. Thermolplastic forming of BMGs has been proved to be a versatile approach by utilizing the superplasticity in SCLR. The understanding of the flow characteristics of the supercooled MGs liquid and the formability under different TPF parameters is crucial in the optimal design of the forming process. The Newtonian flow of MGs during TPF tend to be obtained at the high forming temperature and low strain rate, which has been found to be of benefit to the uniform filling process. Joining BMGs and fabricating micro-/ nanostructures based on TPF have been successfully carried out according to the forming mechanisms in SCLR. However, the issues, such as crystallization,

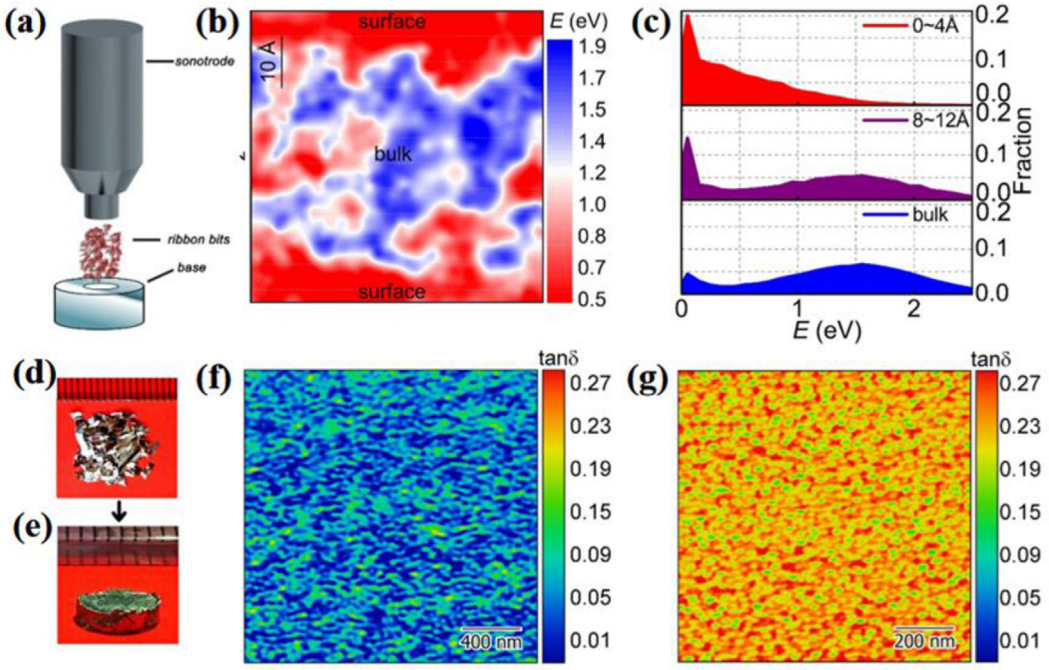

Fig. 13. (a) Schematic diagram of ultrasonic bonding of MGs. (b) Activation energy map of MG surface and (c) its distribution at different distances away from the surface obtained by MD simulation. (d) Photograph of the Zr-based ribbon feedstock and (e) bulk sample fabricated by UPW (diameter: 5 mm; height: 3 mm). (f) The viscoelastic loss tangent map of MG surface under the driving frequency f = 200 Hz and (g) 70,000 Hz (Reprinted from Refs. [34]).

oxidation and thermal diffusion-induced chemical segregation of MGs, still exist and hinder the forming quality by TPF, limiting the process feasibility to the specific composition systems of MGs. A novel forming approach for MGs at room temperature has been developed based on ultrasonic vibration, which can overcome the problems in the thermal process. It is found that MGs can achieve rapid structural rejuvenation and better plasticity under the exertion of high frequency ultrasonic vibration. Based on this, the shear punching and manufacturing processes assisted by ultrasonic vibration have been conducted on different MGs, and the formed parts and multilayer or multiphase MGs have been obtained at ambient temperature, indicating the good versatility of this forming method, while the plastic behavior and fast bonding mechanism of MGs under the high frequency alternating load still need further studies. The forming technologies of MGs have broad prospects in breaking the size limitation of the as-cast MGs, synthesizing new MGs composites, and fabricating sophisticated structures, etc. We expect more fundamental mechanisms and forming approaches of MGs to be discovered and developed in near future to satisfy the diverse applications.

Declaration of competing interest

The authors declare that they have no known competing financial interests or personal relationships that could have appeared to influence the work reported in this paper.

Acknowledgments

The work was supported by the Natural Science Foundation of Guangdong Province (Grant Nr. 2019B030302010), the NSF of China (Grant Nr. 51871157), the Science and Technology Innovation Commission Shenzhen (Grants No. JCYJ20170412111216258), the National Key Research and Development Program of China (Grant No. 2018YFA0703605).

References

[1] W. Wang, Bulk metallic glasses with functional physical properties, Adv. Mater. 21 (2009) 4524–4544.
[2] W. Klement, R. Willens, P. Duwez, Non-crystalline structure in solidified gold–silicon alloys, Nature 187 (1960) 869–870.
[3] N. Nishiyama, K. Amiya, A. Inoue, Novel applications of bulk metallic glass for industrial products, J. Non. Cryst. Solids. 353 (2007) 3615–3621.
[4] A. Inoue, N. Nishiyama, H. Kimura, Preparation and thermal stability of bulk amorphous $Pd_{40}Cu_{30}Ni_{10}P_{20}$ alloy cylinder of 72 mm in diameter, Mater. Trans. JIM. 38 (1997) 179–183.
[5] A. Inoue, A. Takeuchi, Recent development and application products of bulk glassy alloys, Acta Mater. 59 (2011) 2243–2267.
[6] W.-H. Wang, C. Dong, C. Shek, Bulk metallic glasses, Mat. Sci. Eng. R. 44 (2004) 45–89.
[7] N. Nishiyama, K. Takenaka, H. Miura, N. Saidoh, Y. Zeng, A. Inoue, The world's biggest glassy alloy ever made, Intermetallics 30 (2012) 19–24.
[8] D. Turnbull, Under what conditions can a glass be formed? Contemp. Phys. 10 (1969) 473–488.
[9] A. Inoue, T. Zhang, T. Masumoto, Glass-forming ability of alloys, J. Non. Cryst. Solids. 156 (1993) 473–480.
[10] W.L. Johnson, Bulk glass-forming metallic alloys: science and technology, MRS Bull. 24 (1999) 42–56.
[11] P. Lucas, C. Conseil, Z. Yang, Q. Hao, S. Cui, C. Boussard-Pledel, B. Bureau, F. Gascoin, C. Caillaud, O. Gulbiten, Thermoelectric bulk glasses based on the Cu–As–Te–Se system, J. Mater. Chem. A. 1 (2013) 8917–8925.
[12] Y.C. Hu, Y.Z. Wang, R. Su, C.R. Cao, F. Li, C.W. Sun, Y. Yang, P.F. Guan, D.W. Ding, Z.L. Wang, A highly efficient and self-stabilizing metallic-glass catalyst for electrochemical hydrogen generation, Adv. Mater. 28 (2016) 10293–10297.
[13] X. Wang, R. Li, Z. Li, R. Xiao, X.-B. Chen, T. Zhang, Design and preparation of nanoporous Ag–Cu alloys by dealloying Mg–(Ag, Cu)–Y metallic glasses for antibacterial applications, J. Mat. Chem. B. 7 (2019) 4169–4176.
[14] N. Hua, L. Huang, W. Chen, W. He, T. Zhang, Biocompatible Ni-free Zr-based bulk metallic glasses with high-Zr-content: compositional optimization for potential biomedical applications, Mat. Sci. Eng. C. 44 (2014) 400–410.
[15] S. Song, H. Bei, J. Wadsworth, T.-G. Nieh, Flow serration in a Zr-based bulk metallic glass in compression at low strain rates, Intermetallics 16 (2008) 813–818.
[16] Y. Cheng, E. Ma, Atomic-level structure and structure–property relationship in metallic glasses, Prog. Mater. Sci. 56 (2011) 379–473.
[17] C. Pan, T. Wu, M. Chen, Y. Chang, C. Lee, J. Huang, Hot embossing of micro-lens array on bulk metallic glass, Sens. Actuator A-Phys. 141 (2008) 422–431.
[18] Y. Kawamura, T. Shibata, A. Inoue, T. Masumoto, Workability of the supercooled liquid in the $Zr_{65}Al_{10}Ni_{10}Cu_{15}$ bulk metallic glass, Acta Mater. 46 (1998) 253–263.
[19] R. Martinez, G. Kumar, J. Schroers, Hot rolling of bulk metallic glass in its supercooled liquid region, Scr. Mater. 59 (2008) 187–190.
[20] A. Wiest, J.S. Harmon, M.D. Demetriou, R.D. Conner, W.L. Johnson, Injection molding metallic glass, Scr. Mater. 60 (2009) 160–163.
[21] J. Schroers, T.M. Hodges, G. Kumar, H. Raman, A.J. Barnes, Q. Pham, T.A. Waniuk, Thermoplastic blow molding of metals, Mater. Today 14 (2011) 14–19.
[22] L. Liu, M. Hasan, G. Kumar, Metallic glass nanostructures: fabrication, properties, and applications, Nanoscale 6 (2014) 2027–2036.
[23] J. Schroers, On the formability of bulk metallic glass in its supercooled liquid state, Acta Mater. 56 (2008) 471–478.
[24] M. Hasan, G. Kumar, High strain rate thermoplastic demolding of metallic glasses, Scr. Mater. 123 (2016) 140–143.
[25] Q. Zhang, Q.K. Li, M. Li, Chemical segregation in metallic glass nanowires, J. Chem. Phys. 141 (2014) 194701.
[26] W.L. Johnson, G. Kaltenboeck, M.D. Demetriou, J.P. Schramm, X. Liu, K. Samwer, C.P. Kim, D.C. Hofmann, Beating crystallization in glass-forming metals by millisecond heating and processing, Science 332 (2011) 828–833.
[27] G. Kaltenboeck, T. Harris, K. Sun, T. Tran, G. Chang, J.P. Schramm, M.D. Demetriou, W.L. Johnson, Accessing thermoplastic processing windows in metallic glasses using rapid capacitive discharge, Sci. Rep. 4 (2014) 6441.
[28] J. Ma, Z. Huang, H. Zheng, F. Gong, X. Liang, Controllable thermoplastic forming of bulk metallic glasses in milliseconds by resistance welding forming, Mater. Res. Express 6 (2019) 7.
[29] F. Spaepen, A microscopic mechanism for steady state inhomogeneous flow in metallic glasses, Acta Metall. 25 (1977) 407–415.
[30] A. Argon, Plastic deformation in metallic glasses, Acta Metall. 27 (1979) 47–58.
[31] M.L. Falk, J.S. Langer, Dynamics of viscoplastic deformation in amorphous solids, Phys. Rev. E. 57 (1998) 7192.
[32] C. Packard, C. Schuh, Initiation of shear bands near a stress concentration in metallic glass, Acta Mater. 55 (2007) 5348–5358.
[33] J. Pan, Y. Wang, Q. Guo, D. Zhang, A. Greer, Y. Li, Extreme rejuvenation and softening in a bulk metallic glass, Nat. Commun. 9 (2018) 1–9.
[34] J. Ma, C. Yang, X. Liu, B. Shang, Q. He, F. Li, T. Wang, D. Wei, X. Liang, X. Wu, Fast surface dynamics enabled cold joining of metallic glasses, Sci. Adv. 5 (2019), eaax7256.
[35] F. Sun, B. Wang, F. Luo, Y.Q. Yan, H.B. Ke, J. Ma, J. Shen, W.H. Wang, Shear punching of bulk metallic glasses under low stress, Mater. Des. 190 (2020) 108595.
[36] J. Schroers, The superplastic forming of bulk metallic glasses, JOM 57 (2005) 35–39.
[37] J. Schroers, Processing of bulk metallic glass, Adv. Mater. 22 (2010) 1566–1597.
[38] E. Bryn Pitt, G. Kumar, J. Schroers, Temperature dependence of the thermoplastic formability in bulk metallic glasses, J. Appl. Phys. 110 (2011), 043518.
[39] J. Lu, G. Ravichandran, W.L. Johnson, Deformation behavior of the $Zr_{41.2}Ti_{13.8}Cu_{12.5}Ni_{10}Be_{22.5}$ bulk metallic glass over a wide range of strain-rates and temperatures, Acta Mater. 51 (2003) 3429–3443.
[40] J. Qiao, J.M. Pelletier, Crystallization kinetics in $Cu_{46}Zr_{45}Al_7Y_2$ bulk metallic glass by differential scanning calorimetry (DSC), J. Non. Cryst. Solids. 357 (2011) 2590–2594.
[41] S. Lan, X. Wei, J. Zhou, Z. Lu, X. Wu, M. Feygenson, J. Neuefeind, X.L. Wang, In-situ study of crystallization kinetics in ternary bulk metallic glass alloys with different glass forming abilities, Appl. Phys. Lett. 105 (2014) 201906.
[42] C. Peng, Z. Chen, X. Zhao, A. Zhang, L. Zhang, D. Chen, Crystallization kinetics of $Zr_{60}Cu_{25}Fe_5Al_{10}$ bulk metallic glass, J. Non. Cryst. Solids. 405 (2014) 7–11.
[43] N. Li, L. Liu, K. Chan, Q. Chen, J. Pan, Deformation behavior and indentation size effect of $Au_{49}Ag_{5.5}Pd_{2.3}Cu_{26.9}Si_{16.3}$ bulk metallic glass at elevated temperatures, Intermetallics 17 (2009) 227–230.
[44] N. Li, Y. Chen, M. Jiang, D. Li, J. He, Y. Wu, L. Liu, A thermoplastic forming map of a Zr-based bulk metallic glass, Acta Mater. 61 (2013) 1921–1931.
[45] H.M. Chiu, G. Kumar, J. Blawzdziewicz, J. Schroers, Thermoplastic extrusion of bulk metallic glass, Scr. Mater. 61 (2009) 28–31.
[46] J. Ma, L. Huo, D. Zhao, W. Wang, Micro mold filling kinetics of metallic glasses in supercooled liquid state, J. Appl. Phys. 113 (2013) 104505.
[47] N. Li, D. Li, L. Liu, Correlation between flow characteristics and interfacial friction behaviour of a Zr-based metallic glass during micro-extrusion, Philos. Mag. A 93 (2013) 1859–1872.
[48] G. Kumar, H.X. Tang, J. Schroers, Nanomoulding with amorphous metals, Nature 457 (2009) 868–872.
[49] Z. Liu, J. Schroers, General nanomoulding with bulk metallic glasses, Nanotechnology 26 (2015) 145301.

[50] Y. Saotome, K. Itoh, T. Zhang, A. Inoue, Superplastic nanoforming of Pd-based amorphous alloy, Scr. Mater. 44 (2001) 1541–1545.
[51] H. Kato, T. Wada, M. Hasegawa, J. Saida, A. Inoue, H.S. Chen, Fragility and thermal stability of Pt- and Pd-based bulk glass forming liquids and their correlation with deformability, Scr. Mater. 54 (2006) 2023–2027.
[52] Y. Kawamura, Y. Ohno, Spark welding of $Zr_{55}Al_{10}Ni_5Cu_{30}$ bulk metallic glasses, Scr. Mater. 45 (2001) 127–132.
[53] J. Kim, Y. Kawamura, Electron beam welding of the dissimilar Zr-based bulk metallic glass and Ti metal, Scr. Mater. 56 (2007) 709–712.
[54] Y. Kawahito, T. Terajima, H. Kimura, T. Kuroda, K. Nakata, S. Katayama, A. Inoue, High-power fiber laser welding and its application to metallic glass $Zr_{55}Al_{10}Ni_5Cu_{30}$, Mater. Sci. Eng. B. 148 (2008) 105–109.
[55] Y. Kawamura, Liquid phase and supercooled liquid phase welding of bulk metallic glasses, Mater. Sci. Eng. A. 375 (2004) 112–119.
[56] J.J. Lewandowski, W.H. Wang, A.L. Greer, Intrinsic plasticity or brittleness of metallic glasses, Philos. Mag. Lett. 85 (2005) 77–87.
[57] Y. Kawamura, Y. Ohno, Superplastic bonding of bulk metallic glasses using friction, Scr. Mater. 45 (2001) 279–285.
[58] H.S. Shin, J.S. Park, Y.C. Jung, J.H. Ahn, Y. Yokoyama, A. Inoue, Similar and dissimilar friction welding of Zr–Cu–Al bulk glassy alloys, J. Alloy. Compd. 483 (2009) 182–185.
[59] Y. Kawamura, T. Shoji, Y. Ohno, Welding technologies of bulk metallic glasses, J. Non. Cryst. Solids. 317 (2003) 152–157.
[60] T. Shoji, Y. Kawamura, Y. Ohno, Friction welding of bulk metallic glasses to different ones, Mater. Sci. Eng. A. 375 (2004) 394–398.
[61] H.Y. Chen, J. Cao, X.G. Song, G.D. Si, J.C. Feng, Pre-friction diffusion hybrid bonding of $Zr_{55}Cu_{30}Ni_5Al_{10}$ bulk metallic glass, Intermetallics 32 (2013) 30–34.
[62] G. Wang, Y.J. Huang, D. Makhanlall, J. Shen, Friction joining of $Ti_{40}Zr_{25}Ni_3Cu_{12}Be_{20}$ bulk metallic glass, J. Mater. Process. Technol. 212 (2012) 1850–1855.
[63] H. Somekawa, A. Inoue, K. Higashi, Superplastic and diffusion bonding behavior on Zr–Al–Ni–Cu metallic glass in supercooled liquid region, Scr. Mater. 50 (2004) 1395–1399.
[64] H. Somekawa, H. Watanabe, K. Higashi, The grain size dependence on diffusion bonding behavior in superplastic Mg alloys, Mater. Trans. 44 (2003) 496–503.
[65] J.G. Wang, J.C. Fan, Y.F. Zhang, G. Wang, W.H. Wang, K.C. Chan, Diffusion bonding of a Zr-based metallic glass in its supercooled liquid region, Intermetallics 46 (2014) 236–242.
[66] J. Ma, K.C. Chan, L. Xia, S.H. Chen, E.F. Wu, W.H. Li, W.H. Wang, Multi-layer laminated Pd-based metallic glass with enhanced plasticity, Mater. Sci. Eng. A. 587 (2013) 240–243.
[67] G. Kumar, P.A. Staffier, J. Blawzdziewicz, U.D. Schwarz, J. Schroers, Atomically smooth surfaces through thermoplastic forming of metallic glass, Appl. Phys. Lett. 97 (2010) 101907.
[68] W. Chen, Z. Liu, J. Schroers, Joining of bulk metallic glasses in air, Acta Mater. 62 (2014) 49–57.
[69] Q. Peng, Y. Xie, B. Zhu, W. Chen, J. Schroers, M.X. Chen, Z. Liu, Joining mechanism of bulk metallic glasses in their supercooled liquid region, J. Mater. Process. Technol. 279 (2020) 116583.
[70] W. Xu, W. Li, S. Chen, X. Wang, F. Li, Superplastic diffusion bonding of metallic glasses by rapid heating, Intermetallics 98 (2018) 143–147.
[71] Z. Liu, W. Chen, J. Carstensen, J. Ketkaew, R. Miguel, O. Mota, J.K. Guest, J. Schroers, 3D metallic glass cellular structures, Acta Mater. 105 (2016) 35–43.
[72] J.J. He, N. Li, N. Tang, X.Y. Wang, C. Zhang, L. Liu, The precision replication of a microchannel mould by hot-embossing a Zr-based bulk metallic glass, Intermetallics 21 (2012) 50–55.
[73] F. Wang, H. Zhang, X. Liang, F. Gong, J. Ma, Fabrication of metallic glass micro grooves by thermoplastic forming, J. Micromech. Microeng. 27 (2016), 025009.
[74] J.P. Chu, H. Wijaya, C.W. Wu, T.R. Tsai, J. Wadsworth, Nanoimprint of gratings on a bulk metallic glass, Appl. Phys. Lett. 90 (2007), 034101.
[75] J. Ma, J. Yi, D.Q. Zhao, M.X. Pan, W.H. Wang, Large size metallic glass gratings by embossing, J. Appl. Phys. 112 (2012), 064505.
[76] J. Ma, X. Zhang, W.H. Wang, Metallic glass mold insert for hot embossing of polymers, J. Appl. Phys. 112 (2012), 024506.
[77] J.P. Singer, M. Gopinadhan, Z. Shao, A.D. Taylor, J. Schroers, C.O. Osuji, Nanoimprinting sub-100 nm features in a photovoltaic nanocomposite using durable bulk metallic glass molds, ACS Appl. Mater. Inter. 7 (2015) 3456–3461.
[78] J. Padmanabhan, E.R. Kinser, M.A. Stalter, C. Duncan-Lewis, J.L. Balestrini, A.J. Sawyer, J. Schroers, T.R. Kyriakides, Engineering cellular response using nanopatterned bulk metallic glass, ACS Nano 8 (2014) 4366–4375.
[79] E.R. Kinser, J. Padmanabhan, R. Yu, S.L. Corona, J. Li, S. Vaddiraju, A. Legassey, A. Loye, J. Balestrini, D.A. Solly, Nanopatterned bulk metallic glass biosensors, ACS Sens. 2 (2017) 1779–1787.
[80] H.J. Tarigan, N. Kahler, N.S. Ramos, G. Kumar, A.A. Bernussi, Low reflectance of nano-patterned Pt-Cu-Ni-P bulk metallic glass, Appl. Phys. Lett. 107 (2015), 021903.
[81] C. Uzun, C. Meduri, N. Kahler, L.G. de Peralta, J.M. McCollum, M. Pantoya, G. Kumar, A.A. Bernussi, Photoinduced heat conversion enhancement of metallic glass nanowire arrays, J. Appl. Phys. 125 (2019), 015102.
[82] M. Carmo, R.C. Sekol, S. Ding, G. Kumar, A.D. Taylor, Bulk metallic glass nanowire architecture for electrochemical applications, ACS Nano 5 (2011) 2979–2983.
[83] R.C. Sekol, G. Kumar, M. Carmo, F. Gittleson, N. Hardesty-Dyck, S. Mukherjee, J. Schroers, A.D. Taylor, Bulk metallic glass micro fuel cell, Small 9 (2013) 2081–2085.
[84] J. Ma, X.Y. Zhang, D.P. Wang, D.Q. Zhao, D.W. Ding, K. Liu, W.H. Wang, Superhydrophobic metallic glass surface with superior mechanical stability and corrosion resistance, Appl. Phys. Lett. 104 (2014) 173701.
[85] M. Hasan, J. Schroers, G. Kumar, Functionalization of metallic glasses through hierarchical patterning, Nano Lett. 15 (2015) 963–968.
[86] M. Hasan, G. Kumar, High-throughput drawing and testing of metallic glass nanostructures, Nanoscale 9 (2017) 3261–3268.
[87] M. Hasan, N. Kahler, G. Kumar, Shape-controlled metal-metal and metal-polymer Janus structures by thermoplastic embossing, ACS Appl. Mater. Inter. 8 (2016) 11084–11090.
[88] F. Blaha, B. Langenecker, Dehnung von Zink-Kristallen unter Ultraschalleinwirkung, Naturwissenschaften 42 (1955) 556.
[89] B. Langenecker, Effects of ultrasound on deformation characteristics of metals, IEEE Trans. Son. Ultrason. 13 (2005) 1–8.
[90] J.C. Hung, C.C. Lin, Investigations on the material property changes of ultrasonic-vibration assisted aluminum alloy upsetting, Mater. Des. 45 (2013) 412–420.
[91] T. Jimma, Y. Kasuga, N. Iwaki, O. Miyazawa, E. Mori, K. Ito, H. Hatano, An application of ultrasonic vibration to the deep drawing process, J. Mater. Process. Technol. 80 (1998) 406–412.
[92] T. Takemasu, S. Yamasaki, H. Miura, R. Mizue, T. Hoshiyama, T. Ozaki, Piercing process by punch striking using ultrasonic vibration-trial construction of experimental apparatus and forming property of microholes, J. Jap. Soc. Technol. Plast. 47 (2006) 81.
[93] X.J. Hu, X.H. Li, Q.Y. Qin, Influence of ultrasonic vibration on metal plastic forming, Appl. Mech. Mater. 470 (2014) 162–169.
[94] D. She, W. Yue, Z. Fu, Y. Gu, C. Wang, J. Liu, The effect of nitriding temperature on hardness and microstructure of die steel pre-treated by ultrasonic cold forging technology, Mater. Des. 49 (2013) 392–399.
[95] J.C. Hung, C.C. Huang, Evaluation of friction in ultrasonic vibration-assisted press forging using double cup extrusion tests, Int. J. Precis. Eng. Man. 13 (2012) 2103–2108.
[96] H. Qi, X. Shan, T. Xie, Design and experiment of the high speed wire drawing with ultrasound, Chin. J. Mech. Eng. (2009) 580.
[97] G.L. Chern, Y.J.E. Wu, S.F. Liu, Development of a micro-punching machine and study on the influence of vibration machining in micro-EDM, J. Mater. Process. Technol. 180 (2006) 102–109.
[98] H.J. Leamy, T.T. Wang, H.S. Chen, Plastic flow and fracture of metallic glass, Metall. Mater. Trans. B 3 (1972) 699–708.
[99] Y.H. Liu, G. Wang, R.J. Wang, D.Q. Zhao, M.X. Pan, W.H. Wang, Super plastic bulk metallic glasses at room temperature, Science 315 (2007) 1385–1388.
[100] N. Li, X. Xu, Z. Zheng, L. Liu, Enhanced formability of a Zr-based bulk metallic glass in a supercooled liquid state by vibrational loading, Acta Mater. 65 (2014) 400–411.
[101] Han Guangchao, Peng Zhuo, Xu Linhong, Li Ning, Ultrasonic vibration facilitates the micro-formability of a Zr-based metallic glass, Materials 11 (2018) 2568.
[102] Y. Lou, X. Liu, J. He, M. Long, Ultrasonic-assisted extrusion of ZK60 Mg alloy micropins at room temperature, Ultrasonics 83 (2018) 194–202.
[103] Y. Lou, X. Liu, X. Yang, Y. Ge, D. Zhao, H. Wang, L.C. Zhang, Z. Liu, Fast rejuvenation in bulk metallic glass induced by ultrasonic vibration pre-compression, Intermetallics 118 (2020) 106687.
[104] F. Luo, F. Sun, K. Li, F. Gong, X. Liang, X. Wu, J. Ma, Ultrasonic assisted micro-shear punching of amorphous alloy, Mater. Res. Lett. 6 (2018) 545–551.
[105] H. Li, Y. Yan, F. Sun, K. Li, F. Luo, J. Ma, Shear punching of amorphous alloys under high-frequency vibrations, Metals 9 (2019) 1158.
[106] W. Jiao, P. Wen, H. Peng, H.Y. Bai, B.A. Sun, W.H. Wang, Evolution of structural and dynamic heterogeneities and activation energy distribution of deformation units in metallic glass, Appl. Phys. Lett. 102 (2013) 101903.
[107] Z. Wang, P. Wen, L.S. Huo, H.Y. Bai, W.H. Wang, Signature of viscous flow units in apparent elastic regime of metallic glasses, Appl. Phys. Lett. 101 (2012) 121906.
[108] L.S. Huo, J. Ma, H.B. Ke, H.Y. Bai, D.Q. Zhao, W.H. Wang, The deformation units in metallic glasses revealed by stress-induced localized glass transition, J. Appl. Phys. 111 (2012) 113522.
[109] X. Huang, K.J. Hanley, Z. Zhang, C.Y. Kwok, Structural degradation of sands during cyclic liquefaction: insight from DEM simulations, Comput. Geotech. 114 (2019) 103139.
[110] J. Ma, X. Liang, X. Wu, Z. Liu, F. Gong, Sub-second thermoplastic forming of bulk metallic glasses by ultrasonic beating, Sci. Rep. 5 (2015) 17844.
[111] E. Williams, N. Lavery, Laser processing of bulk metallic glass: a review, J. Mater. Process. Technol. 247 (2017) 73–91.
[112] Y. Kawamura, Y. Ohno, Successful electron-beam welding of bulk metallic glass, Mater. Trans. 42 (2001) 2476–2478.
[113] J. Kim, S. Shin, C. Lee, Characterization of the gas tungsten arc welded Cu54Ni6Zr22Ti18 bulk metallic glass weld, Mater. Trans. 46 (2005) 1440–1442.
[114] S. Fukumoto, A. Soeda, Y. Yokoyama, M. Minami, M. Matsushima, K. Fujimoto, Estimation of current path area during small scale resistance

spot welding of bulk metallic glass to stainless steel, Sci. Technol. Weld. Joi. 18 (2013) 135–142.
[115] J.C. Trenkle, T.P. Weihs, T.C. Hufnagel, Fracture toughness of bulk metallic glass welds made using nanostructured reactive multilayer foils, Scr. Mater. 58 (2008) 315–318.
[116] W.D. Liu, K.X. Liu, Q.Y. Chen, J.T. Wang, H.H. Yan, X.J. Li, Metallic glass coating on metals plate by adjusted explosive welding technique, Appl. Surf. Sci. 255 (2009) 9343–9347.
[117] Jonghyun Kim, Weldability of $Cu_{54}Zr_{22}Ti_{18}Ni_6$ bulk metallic glass by ultrasonic welding processing, Mater. Lett. 130 (2014) 160–163.
[118] X. Ma, S.M. Howard, B.K. Jasthi, Friction stir welding of bulk metallic glass Vitreloy 106a, J. Manuf. Sci. Eng. 136 (2014).
[119] S. Kumar, C. Wu, G. Padhy, W. Ding, Application of ultrasonic vibrations in welding and metal processing: a status review, J. Manuf. Process. 26 (2017) 295–322.
[120] S. Yadav, C. Doumanidis, Thermomechanical analysis of an ultrasonic rapid manufacturing (URM) system, J. Manuf. Process. 7 (2005) 153–161.
[121] H. Kreye, M. Hammerschmidt, G. Reiners, Ultrasonic welding of metallic alloy glass to copper, Scr. Metall. 12 (1978) 1059–1061.
[122] 松岡信一, Fe 系及び Ni 系アモルファス合金の超音波接合, 精密機械. 50 (1984) 969-974.
[123] M. Maeda, Y. Takahashi, M. Fukuhara, X. Wang, A. Inoue, Ultrasonic bonding of $Zr_{55}Cu_{30}Ni_5Al_{10}$ metallic glass, Mater. Sci. Eng. B. 148 (2008) 141–144.
[124] M. Maeda, T. Yamasaki, Y. Takahashi, A. Inoue, Interfacial microstructure and thermal stability of $Zr_{55}Cu_{30}Ni_5Al_{10}$ metallic glass joints formed by ultrasonic bonding, Mater. Trans. 50 (2009) 1263–1268.
[125] S. Tamura, Y. Tsunekawa, M. Okumiya, M. Hatakeyama, Ultrasonic cavitation treatment for soldering on Zr-based bulk metallic glass, JJ. Mater. Process. Technol. 206 (2008) 322–327.
[126] H. Nishikawa, K. WongPiromsarn, H. Abe, T. Takemoto, M. Fukuhara, A. Inoue, Solderability of bulk metallic glasses using lead-free solders, Mater. Trans. 50 (6) (2009), 0905150783-0905150783.
[127] H. Ji, L. Li, M. Li, Low-temperature joining of Fe-based amorphous foil with aluminum by ultrasonic-assisted soldering with Sn-based fillers, Mater. Des. 84 (2015) 254–260.
[128] X. Zhang, Y. Xiao, L. Wang, C. Wan, Q. Wang, H. Sheng, M. Li, Ultrasound-induced liquid/solid interfacial reaction between Zn-3Al alloy and Zr-based bulk metallic glasses, Ultrason. Sonochem. 45 (2018) 86–94.
[129] X. Song, Z. Zhu, Y. Chen, Ultrasonic welding of $Fe_{78}Si_9B_{13}$ metallic glass, Mater. Sci. For. 809 (2014) 348–353.
[130] W. Wu, J. Jiang, G. Li, J.Y.H. Fuh, H. Jiang, P. Gou, L. Zhang, W. Liu, J. Zhao, Ultrasonic manufacturing of bulk Ni-based metallic glass, J. Non. Cryst. Solids. 506 (2019) 1–5.
[131] G. Li, J. Zhao, J.Y.H. Fuh, W. Wu, J. Jiang, T. Wang, S. Chang, Experiments on the ultrasonic bonding manufacturing of metallic glass and crystalline metal composite, Materials 12 (2019) 2975.
[132] Y. Wang, Q. Yang, X. Liu, Y. Liu, B. Liu, R.D.K. Misra, H. Xu, P. Bai, Microstructure and mechanical properties of amorphous strip/aluminum laminated composites fabricated by ultrasonic consolidation, Mater. Sci. Eng. A. 749 (2019) 74–78.
[133] C.R. Cao, Y.M. Lu, H.Y. Bai, W.H. Wang, High surface mobility and fast surface enhanced crystallization of metallic glass, Appl. Phys. Lett. 107 (2015) 141606.
[134] H.W. Wei, The elastic properties, elastic models and elastic perspectives of metallic glasses, Prog. Mater. Sci. 57 (2012) 487–656.